



Earth and Space Science

RESEARCH ARTICLE

10.1029/2020EA001276

Key Points:

- Five parameterizations for droplet spectral shape have different impacts on cloud microphysical properties, precipitation, and radiation
- Global dispersion effects caused by the five parameterizations modify the aerosol indirect effect by –10% (counteract) to 13% (strengthen)
- The varying dispersion effects can be explained by different responses of cloud properties in different spectral parameterizations

Correspondence to:

Y. Peng,
pyiran@tsinghua.edu.cn

Citation:

Wang, M., Peng, Y., Liu, Y., Liu, Yu, Xie, X., & Guo, Z. (2020). Understanding cloud droplet spectral dispersion effect using empirical and semi-analytical parameterizations in NCAR CAM5.3. *Earth and Space Science*, 7, e2020EA001276. <https://doi.org/10.1029/2020EA001276>

Received 20 MAY 2020

Accepted 30 MAY 2020

Accepted article online 9 JUN 2020

Author Contributions:

Conceptualization: Minqi Wang, Yiran Peng

Data curation: Yangang Liu, Yu Liu, Xiaoning Xie, Zengyuan Guo

Formal analysis: Minqi Wang, Yangang Liu, Yu Liu, Xiaoning Xie, Zengyuan Guo

Methodology: Minqi Wang, Yiran Peng, Yangang Liu, Yu Liu, Xiaoning Xie, Zengyuan Guo

Writing - original draft: Minqi Wang

Writing - review & editing: Yangang Liu, Yu Liu, Xiaoning Xie, Zengyuan Guo

©2020. The Authors.

This is an open access article under the terms of the Creative Commons Attribution License, which permits use, distribution and reproduction in any medium, provided the original work is properly cited.

Understanding Cloud Droplet Spectral Dispersion Effect Using Empirical and Semi-Analytical Parameterizations in NCAR CAM5.3

Minqi Wang¹ , Yiran Peng¹ , Yangang Liu² , Yu Liu³ , Xiaoning Xie⁴ , and Zengyuan Guo¹

¹Ministry of Education Key Laboratory for Earth System Modeling, Department of Earth System Science, Tsinghua University, Beijing, China, ²Brookhaven National Laboratory, Upton, NY, USA, ³Chinese Academy of Meteorological Sciences, Beijing, China, ⁴SKLLQG, Institute of Earth Environment, Chinese Academy of Sciences, Xi'an, China

Abstract Five parameterizations of cloud droplet spectral shape are implemented in a global climate model to investigate the dispersion effect and aerosol indirect effect (AIE). We design a series of experiments by modifying the microphysical cloud scheme of NCAR CAM5.3 (National Center for Atmospheric Research Community Atmosphere Model Version 5.3). We employ four empirical (Martin94, RLiu03, PengL03, and Liu08) and one semi-analytical (LiuLi15) expressions for cloud droplet spectral shape parameters. Analysis focuses on the instantaneous differences in the simulated cloud microphysical properties and the comparison between model output and satellite data. The results show that RLiu03, PengL03, and LiuLi15 produce wider droplet spectrum and faster autoconversion rate, but Liu08 has a narrower droplet spectrum and slower autoconversion rate than the default parameterization (Martin94) in CAM5.3. Global dispersion effects caused by the five parameterizations modify the aerosol indirect effect by –10% (counteract) to 13% (strengthen). The simulated AIEs and dispersion effects exhibit noticeably spatial inhomogeneity. In the sensitive regions of AIE (Southeast Asia, North Pacific, and West Coast of South America), we decompose the response of shortwave cloud forcing to the change in droplet number for analysis. The varying dispersion effects can be explained by different responses of cloud properties in different spectral parameterizations.

Plain Language Summary Increase of air pollution modifies the water cloud droplet size spectrum and further impacts on cloud physical properties, precipitation, and energy budget in atmosphere. We applied four empirical and one semi-analytical schemes for calculating cloud droplet spectral shape parameters in a global climate model. The five spectral schemes have different impacts on cloud physical properties but have limited effects on global atmospheric energy and on total precipitation. The model simulated changes in cloud properties and in atmospheric energy are analyzed in detail, helping to understand the physical mechanism of the five spectral schemes.

1. Introduction

Aerosols have significant impacts on both microphysical and radiative properties of warm stratiform clouds. The increased aerosol number enhances the cloud droplet number concentration and reduces the size of droplets, cooling the Earth's surface by reflecting more solar radiation, which is called the shortwave aerosol indirect effect (SW AIE) (Twomey, 1991). The increased aerosol number also modifies the shape of cloud droplet size spectrum, which is called dispersion effect. Dispersion effect was originally noticed in aircraft campaigns. Liu and Daum (2002) comprehensively analyzed the aircraft measurements of cloud droplet size-number spectrum in coastal stratus and stratocumulus clouds, and first pointed out the importance of dispersion effect in climate studies.

In the twentieth century, the spectral shape of cloud droplet spectrum in most global climate models (GCMs) was adopted the simplest way to set to a constant. It means the droplet spectral shape would not change as clouds evolve and the dispersion effect was completely ignored. In the first decade of the 21st century, parameterizations of spectral shape were introduced into GCMs to represent the influence of aerosols on cloud droplet spectrum, which made the estimation of dispersion effect and its impact on cloud radiation possible (e.g., Rotstayn & Liu, 2009; Xie et al., 2017, 2018). Several empirical formulas have been developed by fitting

to the aircraft observations and exhibited a broader spectrum with increased cloud droplet number concentration (i.e., positive dispersion effect). The shortwave cooling effect induced by increasing aerosol number can be partially offset by the positive dispersion effect in GCMs (Peng & Lohmann, 2003; Rotstayn & Liu, 2003).

In the past two decades of 21st century, a large number of cloud observations confirmed the strong correlation between an effective radius factor (β , higher value of β means a wider spectrum) and cloud droplet number concentration (N_d) for stratus/stratocumulus clouds. However, both positive (Liu & Daum, 2002; Martin et al., 1994; Peng & Lohmann, 2003; Rotstayn & Liu, 2003) and negative (Lu et al., 2007; Ma et al., 2010; Martins & Dias, 2009) $\beta - N_d$ relationships have been identified in abundant cloud measurements. A few observations even show that β initially increases and decreases afterward with the increased aerosol during the growing stage of clouds (Wang et al., 2019). The contradictory and complex relationships of $\beta - N_d$ indicate that the shape of cloud droplet spectrum is not only related to aerosols but also affected by other factors.

Updraft is another major factor that affects the dispersion effect. Based on theoretical derivation, β is inversely correlated with the updraft velocity under the adiabatic condition (Liu et al., 2006). Studies with an adiabatic parcel model (Chen et al., 2016, 2018; Liu et al., 2014) indicate that opposite $\beta - N_d$ relationships exhibit in aerosol-limited and updraft-limited regimes, respectively, confirming the dependence of droplet spectral shape on updraft velocity. According to the observational and theoretical analyses, Liu et al. (2008) introduced liquid water content (Q_c) into the parameterization of spectral shape, as they found cloud updraft should have much less impact on $\beta - Q_c/N_d$ relationship than on $\beta - N_d$ relationship (Liu et al., 2006). Liu and Li (2015) developed a semi-analytical method to parameterize the droplet spectral shape by solving the condensational equation, implicitly including the impact of updraft velocity on the condensational growth of cloud droplets. However, the semi-analytical parameterization has not been implemented in GCMs nor compared with the earlier empirical parameterizations with positive $\beta - N_d$ relationship. The simulated dispersion effect and SW AIE with the different spectral shape parameterizations need to be investigated, too.

This research focuses on understanding empirical and semi-analytical parameterizations of cloud droplet spectral shape, analyzing their impacts on cloud microphysical properties, radiative fluxes, and precipitation and also quantifying the dispersion effect and the aerosol indirect effect in a GCM. This paper is organized as follows. Section 2 introduces the parameterizations applied in model and calculation methods we used. Section 3 shows the GCM simulation results and the analysis of SW AIE and dispersion effect. Section 4 presents the concluding remarks.

2. Methods

2.1. Model Description

In this study, all the simulations are performed with the stand-alone Community Atmosphere Model version 5.3 (CAM5.3). Climatological sea surface temperature (SST) and sea ice provided by Hadley Center as monthly means averaged over 1981–2001 are used to drive the model repeatedly. Greenhouse gas concentrations are fixed, and carbon dioxide is set to 367 ppm (Neale et al., 2012). Two emission scenarios of aerosols and precursor gases are adopted to represent the preindustrial (PI, year 1850) and the present day (PD, year 2000), respectively, anthropogenic sources of primarily emitted sulfate, black carbon and organic aerosol, and precursor gases are substantially increased from PI to PD. The 7-mode Modal Aerosol Module (MAM7) is used for aerosol simulation in CAM5.3. MAM7 avoids the instantaneous internally mixing of primary carbonic aerosols and includes the detailed divisions of mixing state and size distribution for dust and sea salt (Liu et al., 2012). Shortwave and longwave radiative transfer calculations are performed by using the Rapid Radiative Transfer Model for General circulation model applications (Iacono et al., 2008; Mlawer et al., 1997). Two-moment microphysical scheme (MG1.5 scheme) is adopted into CAM5.3 to predict the variance of cloud water and droplet number concentration for stratiform/stratus clouds (Gettelman et al., 2008; Morrison & Gettelman, 2008). Both PI and PD simulations are integrated for 6 years, and the last 5-year results are analyzed in this study.

2.1.1. Droplet Spectral Shape and Effective Radius

In CAM5.3, soluble aerosol particles (including sulfate, sea salt, aged black carbon and organic aerosol, and dust coated with sulfate) can be activated to form cloud droplets. The activation of aerosols and the subsequent droplet growth by vapor condensation are calculated depending on aerosol properties (size, number, solubility, etc.) and environmental variables (updraft and humidity) (Abdul-Razzak & Ghan, 2000).

Number concentration of cloud droplets and cloud liquid water content are two prognostic variables in MG1.5 microphysics scheme for warm stratus clouds. The ratio of third moment to second moment of cloud droplet size-number spectrum is defined as the effective radius of cloud droplets (R_e), which is important for subsequent calculations of cloud radiation properties and cloud-to-rain conversion. The effective radius is diagnosed in MG1.5 scheme as the product of effective radius factor (β) and volume mean radius of cloud droplets (R_v).

$$R_e = \beta \times R_v. \quad (1)$$

To explicitly define the shape of cloud droplet size-number spectrum, a shape parameter, relative dispersion (ε), is introduced as the ratio of the droplet spectral standard deviation (σ) to the mean radius (R_n).

$$\varepsilon = \sigma / R_n. \quad (2)$$

The cloud droplet spectrum in MG1.5 scheme is approximated by Gamma distribution, which can be represented as

$$n(r) = N_0 r^\mu e^{-\lambda r}, \quad (3)$$

where $n(r)$ is cloud droplet number concentration in a unit volume of unit radius, r is droplet radius, N_0 is intercept, λ is slope, and μ is shape factor (Morrison & Gettelman, 2008).

With the assumption of Gamma distribution for droplet size spectrum, the three shape parameters (shape factor μ , relative dispersion ε , and effective radius factor β) are related to one another through the following equations:

$$\mu = \frac{1}{\varepsilon^2} - 1 \quad (4)$$

or

$$\beta = \frac{(\mu+3)^{2/3}}{[(\mu+2)(\mu+1)]^{1/3}} = \frac{(1+2\varepsilon^2)^{2/3}}{(1+\varepsilon^2)^{1/3}}. \quad (5)$$

Mathematical derivations can be found in Liu and Li (2015) and Liu and Daum (2000).

As mentioned in section 1, effective radius factor β was assigned as constant in earlier GCMs, implicitly assuming no aerosol effect on cloud droplet spectral shape. According to Rotstayn and Liu (2009), $\beta = 1.1$ was often used as a global mean in GCMs. A fixed value of $\beta = 1.145$ (i.e., $\varepsilon = 0.4$) from cloud measurements (Zhao et al., 2006) was applied in Xie et al., (2017). In this study, we employ a fixed $\beta = 1.145$ and also investigate five parameterizations of droplet spectral shape (Table 1). Four of them are empirical and LiuLi15 is semi-analytical. The dependence of β on N_d and Q_c are schematically drawn in Figure 1. For all the parameterization schemes, cloud droplet spectrum broadens as N_d increases (Figure 1a). Q_c implies the influence of cloud dynamic factor on droplet spectrum to a certain degree, which is explicitly considered in Liu08, yet implicitly considered in LiuLi15 (In Figure 1, condensation rate dQ_c/dt is diagnosed with the calculated supersaturation in MG1.5.). Figure 1b shows that Liu08 and LiuLi15 have opposite $\beta - Q_c$ relationships. The cloud droplet spectrum is narrowed as Q_c increases in Liu08 scheme. But the semi-analytical scheme LiuLi15 exhibits a positive $\beta - Q_c$ relationship.

2.1.2. Autoconversion

Precipitation in warm cloud is initiated by the autoconversion process of cloud droplets to raindrops. An empirical parameterization (KK2000, see Table 1) is applied for calculating the autoconversion rate (T) in model. KK2000 employed the regression of N_d and Q_c in a bulk approach (which prescribed a priori shape

Table 1
The Parameterizations of Spectral Shape and Autoconversion

Spectral shape	Formulas	References
Martin94	$\varepsilon = 0.000574N_d + 0.2714$	Martin et al. (1994)
RLiu03	$\varepsilon = 1 - 0.7e^{-0.003N_d}$	Rotstain and Liu (2003)
PengL03	$\beta = 1.18 + 0.00045N_d$	Peng and Lohmann (2003)
Liu08	$\beta = 0.07\left(\frac{Q_c}{N_d}\right)^{-0.14}$	Liu et al. (2008)
LiuLi15	$\mu = \frac{-3 - \sqrt{9 - 8(1 - R_v^3/R_n^3)}}{2(1 - R_v^3/R_n^3)} - 1$	Liu and Li (2015)
Autoconversion	Formulas	References
KK2000	$P = 1350(Q_c \times 10^{-3}/\rho_a)^{2.47} N_d^{-1.79}$	Khairoutdinov and Kogan (2000)
LiuXie	$P = P_0 T; T = \frac{1}{2}(x_c^2 + 2x_c + 2)(1 + x_c)e^{-2x_c}$ $P_0 = 1.1 \times 10^{10} \left[\frac{(1 + 3\varepsilon^2)(1 + 4\varepsilon^2)(1 + 5\varepsilon^2)}{(1 + \varepsilon^2)(1 + 2\varepsilon^2)} \right] N_d^{-1} (Q_c \times 10^{-6})^3 \times 10^3 / \rho_a$	Liu et al. (2005); Xie et al. (2013)

Note. ε is relative dispersion, β is effective radius factor, μ is shape factor, N_d is cloud droplet number concentrations (cm^{-3}), Q_c is liquid water content (g/m^3), R_v is volume mean radius of cloud droplets (μm), R_n is mean radius (μm), ρ_a is air density (kg/m^3), P is autoconversion rate (kg/kg/s), P_0 is rate function, T is threshold function, and $x_c = 9.7 \times 10^{-17} N_d^{3/2} (Q_c \times 10^{-6})^{-2}$

of cloud droplet spectrum as Gamma distribution) to best fit the autoconversion rate derived from large eddy simulation (LES) with explicit spectral bin (droplet spectrum resolving) microphysical model. KK2000 is the default parameterization used in CAM5.3, but it does not explicitly include the dependence of droplet spectral shape on N_d and/or Q_c in model.

Therefore, we introduce another parameterization of autoconversion rate (LiuXie; see Table 1) (Liu et al., 2005; Xie et al., 2013), which consists of two steps calculation (P_0 and T). P_0 represents the conversion rate after the onset of autoconversion process (called rate function hereafter), and T represents the threshold function describing the size truncation effect. Rate function is derived from the continuous collection

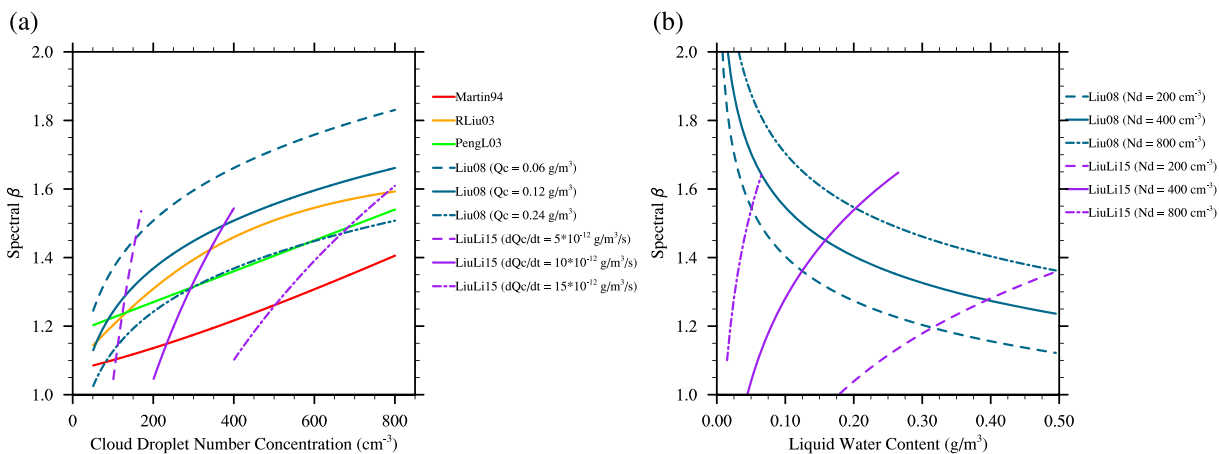


Figure 1. Relationship of effective radius factor (β) to (a) cloud droplet number concentrations (N_d) and (b) liquid water content (Q_c) for the five parameterizations. (a) Red, Martin94; orange, RLiu03; green, PengL03; blue, Liu08 with different Q_c conditions (dashed line: $Q_c = 0.06 \text{ g/m}^3$, solid line: $Q_c = 0.12 \text{ g/m}^3$, pecked line: $Q_c = 0.24 \text{ g/m}^3$); purple, LiuLi15 with different water vapor condensation rate (dQ_c/dt) at 0.1% supersaturation and $Q_c = 0.06 \text{ g/m}^3$ (dashed line: $dQ_c/dt = 5 \times 10^{-12} \text{ g/m}^3/\text{s}$, solid line: $dQ_c/dt = 10 \times 10^{-12} \text{ g/m}^3/\text{s}$, pecked line: $dQ_c/dt = 15 \times 10^{-12} \text{ g/m}^3/\text{s}$). (b) Blue, Liu08 with different N_d (dashed line: $N_d = 200 \text{ cm}^{-3}$, solid line: $N_d = 400 \text{ cm}^{-3}$, pecked line: $N_d = 800 \text{ cm}^{-3}$); purple, LiuLi15 with different N_d (dashed line: $N_d = 200 \text{ cm}^{-3}$, solid line: $N_d = 400 \text{ cm}^{-3}$, pecked line: $N_d = 800 \text{ cm}^{-3}$). Formulas of the five parameterizations are listed in Table 1.

Table 2
Setup of Five Experiments With Different Parameterizations of Droplet Spectral Shape in PD Simulation

Experiments	Spectral param. for feedback run	Spectral param. for no feedback run	Autoconversion param.
Martin94	Martin94	n/a	LiuXie
RLiu03	RLiu03	Martin94	LiuXie
PengL03	PengL03	Martin94	LiuXie
Liu08	Liu08	Martin94	LiuXie
LiuLi15	LiuLi15	Martin94	LiuXie

equation, where larger droplets with higher settling velocities collect smaller droplets (Liu & Daum, 2004). Cloud droplet spectral shape parameter (ε) is explicitly included in LiuXie scheme. In this study, we replace KK2000 with LiuXie scheme, so that the droplet spectral shape parameter is explicitly considered in cloud-to-rain conversion. Compared to KK2000, LiuXie scheme together with an empirical spectral shape parameterization (RLiu03) shows a decrease in autoconversion rate in the upper troposphere and an increase at the lower level (Figure 1 in Xie et al., 2018). The resulted cloud microphysical properties, precipitation, and radiative properties are still within the range of available observations (Table 1 in Xie et al., 2018).

2.2. Methods of Analysis

2.2.1. Double Calls

For PD simulation with CAM5.3, the cloud microphysics scheme (MG1.5) including the spectral shape parameterization in Table 1 and the replaced autoconversion scheme LiuXie is double called in each experiment (see Table 2). For the first call of each experiment, Martin94 (the default parameterization for spectral shape in CAM5.3) is employed and the changes of cloud microphysical variables are diagnosed but not transmitted to the next time step, which is called no feedback run. For the second call, an alternative parameterization for spectral shape (RLiu03, PengL03, Liu08, and LiuLi15 respectively) is employed and the microphysical changes are allowed to influence the climate, which is called feedback run (Table 2). The approach of double calls keeps the same atmospheric conditions in each experiment when calling the two different spectral shape parameterizations in MG1.5, yet allowing for the atmospheric feedback to the individual parameterization of droplet spectral shape. By comparing the instantaneous output of cloud microphysical properties between the feedback run and no feedback run in each experiment, the instantaneous effect of different spectral parameterizations on cloud properties can be identified. Results of feedback runs in the five experiments are also analyzed for investigating the dispersion effect on radiation and precipitation. For PD simulation, both feedback and no feedback runs are conducted to obtain the instantaneous output of cloud properties and present in section 3.1. For PI simulation, only feedback runs are conducted, so that we can derive the SW AIE with each spectral parameterization by including feedback on climate.

2.2.2. Nudging Technique

Nudge (also called Newtonian relaxation) as an assimilation technique is applied in this study to reduce the natural variability of model and to estimate SW AIE by constraining both PD and PI simulations toward the same meteorological conditions (Kooperman et al., 2012). The implementation of nudging in CAM5.3 follows the strategy suggested by Zhang et al. (2012), in which atmospheric horizontal winds are nudged but temperature is released. The prescribed wind fields are taken from the PD simulation of each experiment for feedback run (see Table 2) and apply for PI simulation with the corresponding spectral shape parameterization. With this approach, the meteorology is well constrained while the atmospheric temperature and cloud physics are allowed to rapidly adjust to the aerosol forcing (Forster et al., 2016).

2.2.3. Data Sets for Validation

Multiple satellite observations are used for model validation in this study. We employ the data from International Satellite Cloud Climatology Project (ISCCP) for liquid water path; the Moderate-Resolution Imaging Spectroradiometer (MODIS) level-2v (L2) cloud products for droplet effective radius; the data from Tropical Rainfall Measuring Mission (TRMM) and Global Precipitation Climatology Project (GPCP) for total precipitation; and data from Clouds and the Earth's Radiant Energy System (CERES) for liquid water path, effective radius of cloud droplets, cloud optical depth, and shortwave cloud forcing at top of the atmosphere (TOA). The observational droplet number concentration over the whole cloud profile $N_{d,\text{pro}}$ is diagnosed from CERES cloud optical depth and droplet effective radius according to Painemal and Zuidema (2011):

$$N_{d,\text{pro}} = 1.4067 \times 10^{-6} \cdot \frac{\tau^{\frac{1}{2}}}{R_e^2}. \quad (6)$$

For comparing to the observed $N_{d,\text{pro}}$ derived from CERES data, the simulated $N_{d,\text{pro}}$ is also weighted by the cloud optical depth from cloud top to cloud base.

2.2.4. Decomposition of SW AIE

The enhanced anthropogenic aerosol amount from PI to PD modifies cloud microphysical and radiative properties, exerting SW radiative forcing on the global energy budget (e.g., SW AIE). In model estimates, radiative forcing caused by the change in a cloud physical quantity can be expressed as a format of $d\ln X/d\ln Y$, which can be further decomposed following the relationships below (Ghan et al., 2016):

$$\frac{\Delta \ln \bar{R}_{sw,TOA}}{\Delta \ln \bar{N}_{d,pro}} = \frac{\Delta \ln \bar{C}}{\Delta \ln \bar{N}_{d,pro}} + \frac{\Delta \ln \bar{R}_c}{\Delta \ln \bar{\tau}} \left(\frac{\Delta \ln \bar{L}}{\Delta \ln \bar{N}_{d,pro}} - \frac{\Delta \ln \bar{R}_{e,top}}{\Delta \ln \bar{N}_{d,pro}} \right), \quad (7)$$

$$\frac{\Delta \ln \bar{R}_{sw,TOA}}{\Delta \ln \bar{N}_{d,pro}} = \frac{\Delta \ln \bar{C}}{\Delta \ln \bar{N}_{d,pro}} + \frac{\Delta \ln \bar{R}_c}{\Delta \ln \bar{\tau}} \frac{\Delta \ln \bar{\beta}_{top}}{\Delta \ln \bar{N}_{d,pro}} \left(\frac{\Delta \ln \bar{L}}{\Delta \ln \bar{\beta}_{top}} - \frac{\Delta \ln \bar{R}_{e,top}}{\Delta \ln \bar{\beta}_{top}} \right), \quad (8)$$

where overbars denote quantities averaged over a time period long enough for clouds to adjust to the aerosol enhancement and Δ denotes the difference between the two model simulations (e.g., PD and PI). Change in the shortwave cloud radiative forcing ($R_{sw,TOA}$) can be decomposed to change in cloud fraction (C) and change of the cloud radiative forcing in the cloudy part of the sky (R_c). Change in cloud optical depth (τ) is further decomposed into contributions from changes in cloud liquid water path (L) and R_e by considering the common expression for cloud optical depth $\tau \propto L/R_e$ (Equation 7, which is the same as Equations 7 and 8 in Ghan et al., 2016). Following the same procedure, we include the contribution

from spectral shape parameter β_{top} in Equation 8. We consider that $\frac{\Delta \ln \bar{\beta}_{top}}{\Delta \ln \bar{N}_{d,pro}}$ represents the dispersion effect of aerosol on cloud droplet spectral shape. To quantify the different contributions to SW AIE in section 3.2, $N_{d,pro}$ is weighted by the cloud optical depth as mentioned in section 2.2.3. β_{top} and $R_{e,top}$ are sampled only from the top level of warm clouds in model, because the incoming solar radiative flux and satellite retrieval are more susceptible to droplet size in cloud top than in the lower part of cloud. These cloud microphysical quantities are used when liquid cloud fraction and liquid water both exist in model.

3. Results

3.1. PD Run Results

Figure 2 shows the cloud microphysical properties (β , R_v , R_e , N_d , and Q_c) in five experiments (see Table 2) and the instantaneous difference among the five parameterizations of spectral shape. Since the positive relationship of $\beta - N_d$ is revealed in all parameterizations (Figure 1a), the regions with higher N_d correspond to larger β (Figures 2a1–2e1 and 2a5–2e5). For Liu08, β becomes smaller in the regions with larger Q_c and smaller N_d (Figures 2d1, 2d4, and 2d5), in accordance with the negative correlation between β and Q_c as in Figure 1b. For LiuLi15, larger β occurs in the Southern Hemisphere than in the Northern Hemisphere. Yum and Hudson (2005) pointed out that the growth rate of cloud droplets depends partly on the droplet size; the larger droplets have less efficient condensational growth than smaller droplets. Therefore the overall larger cloud droplets in the southern hemisphere have slower growth rate and wider cloud droplet spectrum (Figure 2e1).

Figure 2 exhibits a range of β values for different droplet spectral shape parameterizations (Figures 2a1–2e1). It is mainly attributed to the different prescribed factors in empirical formulas, that is, the background value of β when N_d is approaching to the lower limit in clouds. For example, in Martin94 and PengL03 the background value of β must be greater than 1.07 (i.e., $\varepsilon = 0.27$) and 1.18, respectively (see formulas in Table 1). In Liu08, the background value of β approaches to 1 when N_d is low. Therefore, β exhibits a certain variation among the five parameterizations (Figures 2a1–2e1).

The lower four rows of Figure 2 present the instantaneous differences in cloud microphysical properties between the alternative parameterization (RLiu03, PengL03, Liu08, or LiuLi15) and the default parameterization (Martin94) of droplet spectral shape. Instantaneous outputs are obtained by double calling the microphysical scheme MG1.5 (as described in section 2.2.2). RLiu03, PengL03, and LiuLi15 produce larger β , larger R_e , and smaller in-cloud Q_c comparing to Martin94. As the wider cloud droplet spectrum makes it easier for cloud droplets to collide each other and grow to raindrop, Q_c and N_d decrease with increased β .

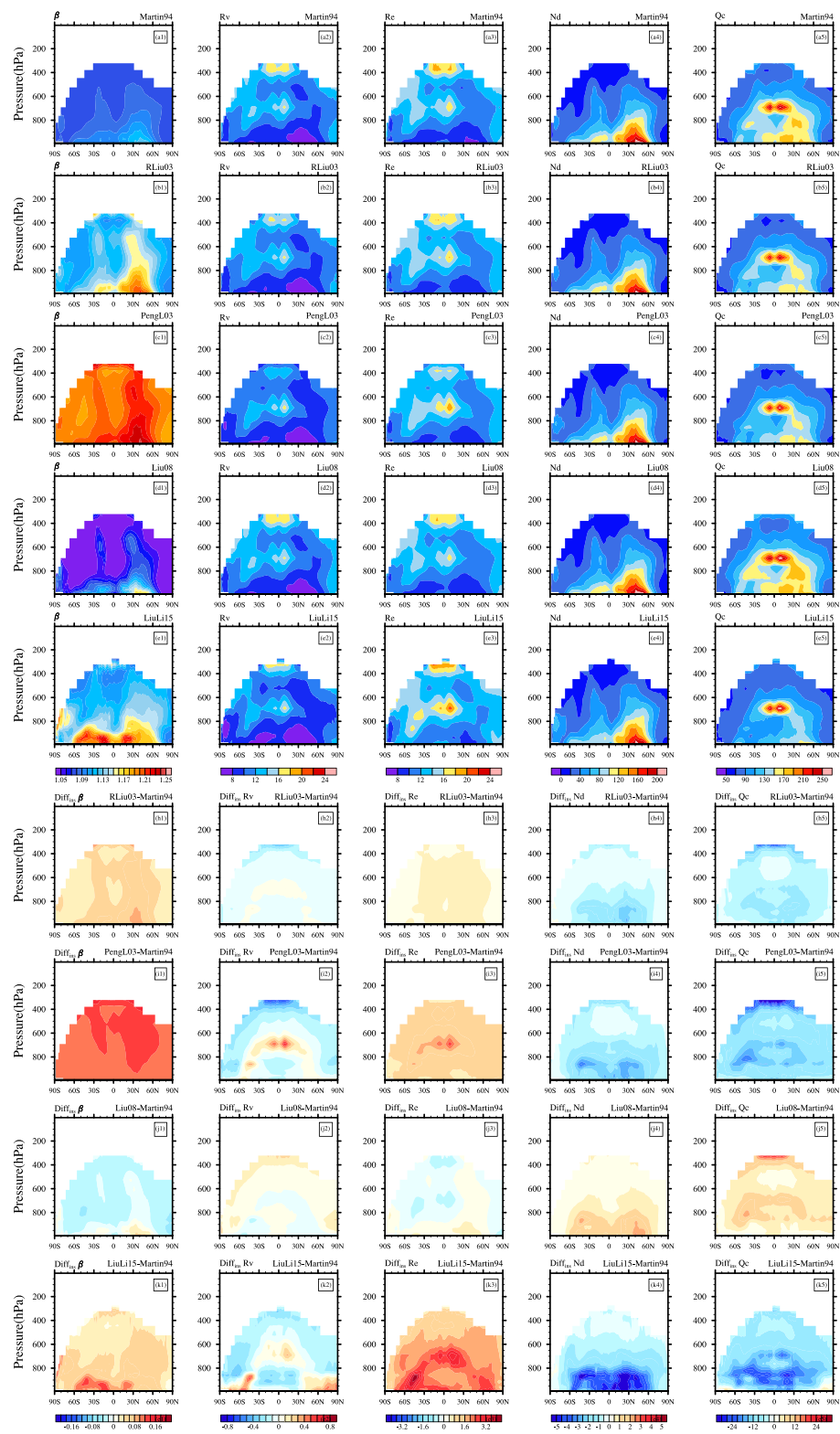


Figure 2. The PD simulation of cloud microphysical variables (effective radius factor β , volume mean radius of cloud droplets R_v , effective radius of cloud droplets R_e , cloud droplet number concentrations N_d , and in-cloud liquid water content Q_c) with different cloud droplet spectral parameterizations (Martin94, RLiu03, PengL03, Liu08, and LiuLi15 as in Table 1) (panels a–e in upper five rows). Instantaneous difference ($\text{Diff}_{\text{ins}} \beta$, $\text{Diff}_{\text{ins}} R_v$, $\text{Diff}_{\text{ins}} R_e$, $\text{Diff}_{\text{ins}} N_d$, and $\text{Diff}_{\text{ins}} Q_c$) between the alternative parameterization of spectral shape (RLiu03, PengL03, Liu08, and LiuLi15) and Martin94 (default parameterization in CAM5.3) (panels f–k in lower four rows).

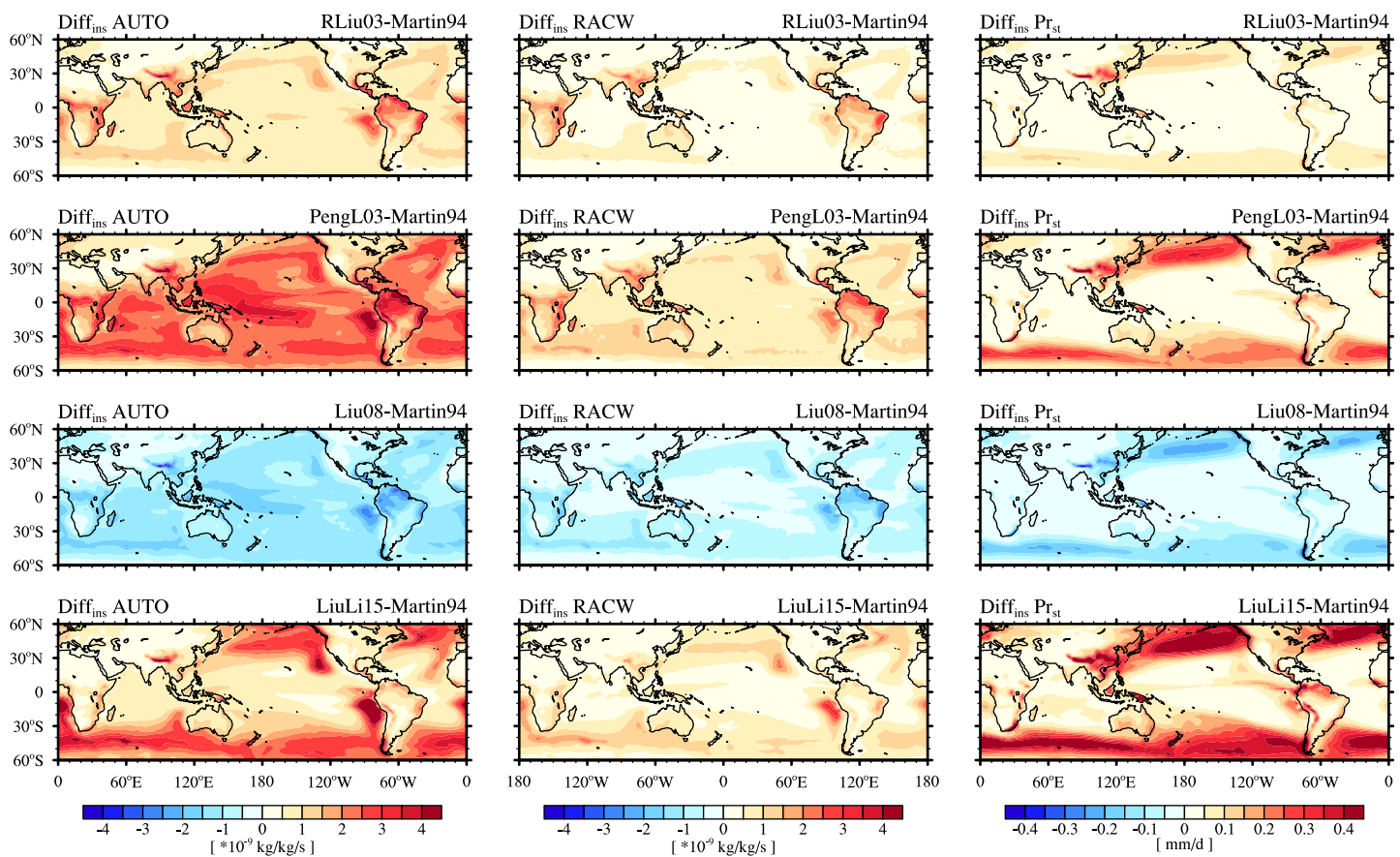


Figure 3. Instantaneous difference in the autoconversion rate ($\text{Diff}_{\text{ins}} \text{ AUTO}$), the accretion of droplets by rain ($\text{Diff}_{\text{ins}} \text{ RACW}$) and stratiform precipitation ($\text{Diff}_{\text{ins}} \text{ Pr}_{\text{st}}$) between the alternative parameterizations of spectral shape (RLiu03, PengL03, Liu08, and LiuLi15) and Martin94 (default parameterization in CAM5.3), respectively.

On the opposite, Liu08 produces smaller β (e.g., narrower cloud droplet spectrum), enhanced Q_c , and N_d than Martin 94 (Figures 2j1, 2j4, and 2j5).

The dispersion effect on autoconversion process is considered by applying LiuXie autoconversion scheme (Table 1 and section 2.1.2). Among all the cloud microphysical processes in MG1.5, autoconversion and accretion of droplets have major impacts on the tendencies of cloud water, cloud droplet number, and stratiform precipitation (not shown). Therefore, Figure 3 shows the instantaneous differences in autoconversion rate and accretion rate between RLiu03, PengL03, Liu08, LiuLi15, and Martin94, respectively, to understand the dispersion effect on formation of stratiform precipitation. RLiu03, PengL03, and LiuLi15 produce wider cloud droplet spectrum than Martin94, which leads to more efficient autoconversion of cloud droplets to raindrops, and more stratiform precipitation formed (rows 1, 2, and 4 in Figure 3). On the contrary, Liu08 has a narrower cloud droplet spectrum, slower autoconversion, and less stratiform precipitation than Martin94 (row 3 in Figure 3). The accretion of droplets by rain is increased when more raindrops are formed by the faster autoconversion rate and vice versa.

In Figure 4 we compare the diagnosed cloud properties with satellite observations for verification. Satellite retrieved cloud data have large uncertainties in the Polar regions; thus, we focus on the comparison between 60°S and 60°N only (Komurcu et al., 2014). To match the observed quantities from satellite retrieval, $N_{d,\text{pro}}$ is obtained by weighting N_d with cloud optical depth in each cloudy layer, to indicate the droplet number concentration over the whole cloud profile (from cloud base to cloud top). L is liquid water path and $R_{e,\text{top}}$ is sampled in the top level of warm clouds in the model. Figure 4a shows that all simulated $N_{d,\text{pro}}$ are overestimated near the tropics and in 30–60°N. L is underestimated in midlatitude regions of storm track for all the spectral shape parameterizations, especially for the parameterizations (LiuLi15, PengL03, and RLiu03) with

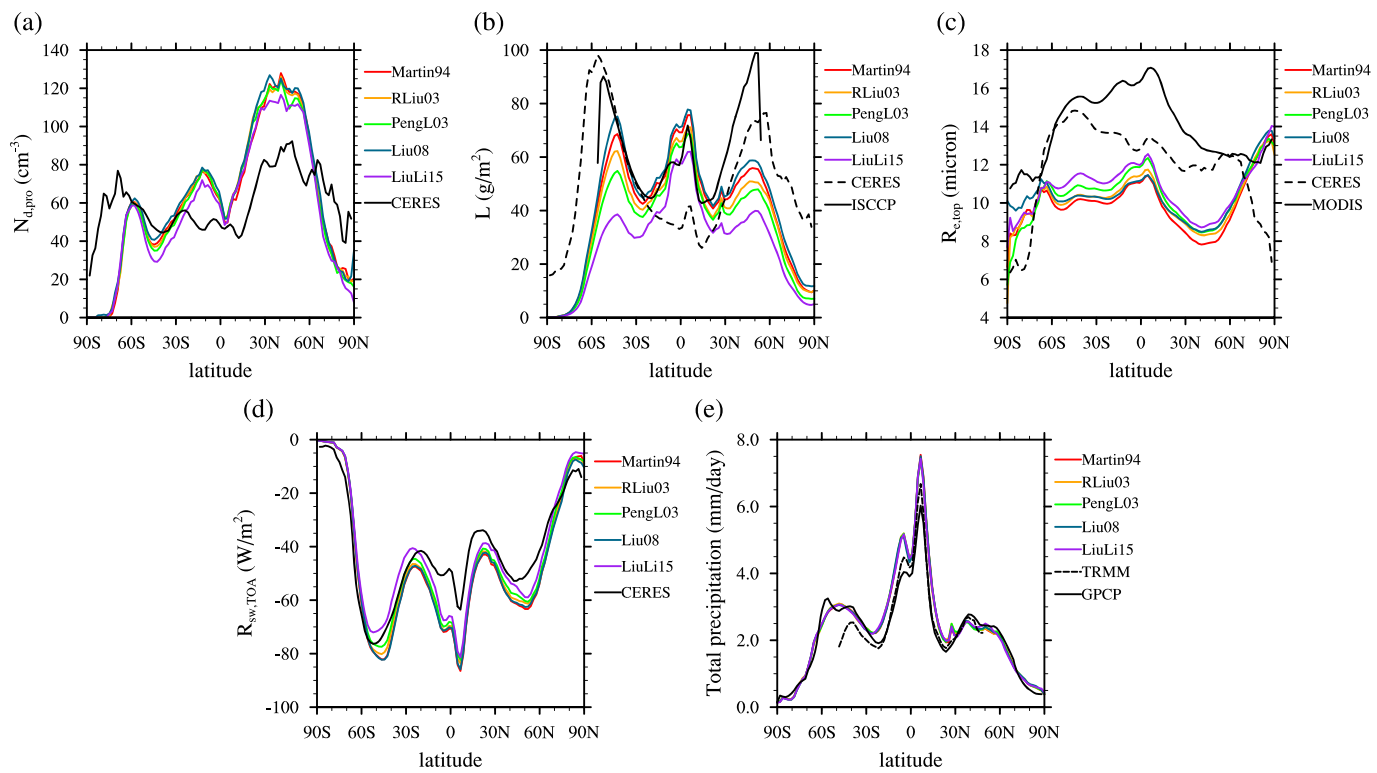


Figure 4. Comparison between model diagnosed outputs and corresponding satellite observations: (a) cloud droplet number concentrations over the cloud profile ($N_{d,\text{pro}}$), (b) liquid water path (L), (c) droplet effective radius in cloud top ($R_{e,\text{top}}$), (d) shortwave cloud forcing at top of the atmosphere ($R_{\text{sw}, \text{TOA}}$), and (e) total precipitation. Red, Martin94; orange, RLiu03; green, PengL03; blue, Liu08; purple, LiuLi15; and black, observations from satellite retrievals of CERES, ISCCP, MODIS, TRMM, and GPCP.

relatively wider cloud droplet spectrum (Figure 4b). The simulated $R_{e,\text{top}}$ is 1 to 4 μm lower than the observations, which is resulted from the overestimation of $N_{d,\text{pro}}$, underestimation of L , and underestimated dispersion (Figure 4c). In Figure 4d, the simulated SW cloud forcing (changes in TOA SW net radiative flux between the PD simulations with and without clouds) exerts stronger cooling near the tropics and midlatitudes than observation, despite the different spectral shape parameterizations. Note that the semi-analytical parameterization LiuLi15 exerts the weakest SW cloud forcing among all the five spectral shape parameterizations, mostly attributed to the lowest L . The results suggest that the overall bias in SW cloud radiative forcing at TOA is hard to be compensated by applying these spectral shape parameterizations tested. Figure 4e shows the comparison of simulated and observed total precipitation. Since the stratiform precipitation contributes modestly to the total precipitation, different spectral parameterizations have negligible impacts on the total precipitation.

3.2. SW AIE and Dispersion Effect

In this section, our analysis focuses on the model estimated SW AIE, the differences in SW cloud forcing between PD and PI simulations. Figure 5 shows the simulated SW AIE by using the fixed $\beta = 1.145$ and the five droplet spectral parameterizations, respectively. The averaged SW AIE over the globe, over land, and over ocean are listed in Table 3. In Figure 5, no matter which spectral parameterization is used in CAM5.3, noticeable SW AIE always occurs in three regions including Southeast Asia (60–130°E; 10°S–20°N), North Pacific region (140°E–120°W; 20–50°N), and West Coast of South America (100°W–80°W; 10°S–5°N). The three regions are downwind aerosol source regions (Southeast Asia, East Asia, and Amazon), and oceans provide abundant moisture for cloud development, thus are regarded as sensitive regions for AIE of liquid clouds in this study (similar to the sensitive regimes identified with satellite data by Zhao et al., 2018). The averaged SW AIEs over the three sensitive regions with each spectral parameterization are listed in Table 3, too.

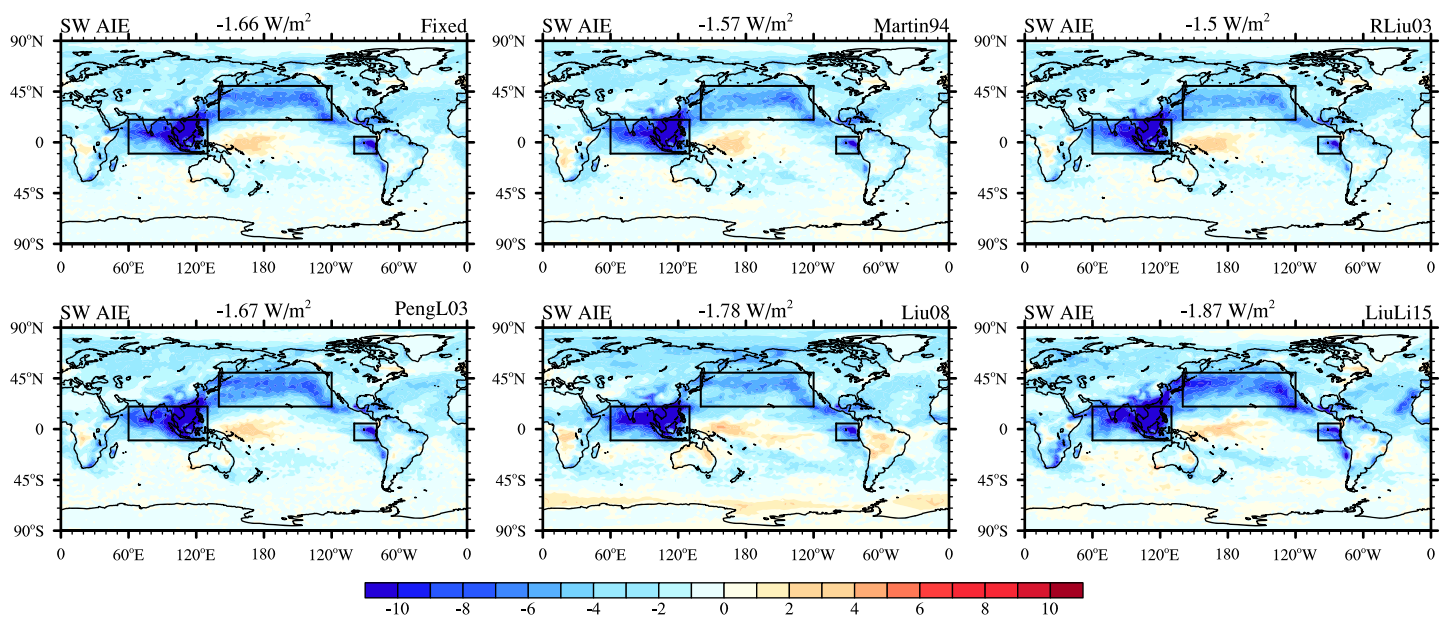


Figure 5. Simulated SW AIE (unit is W/m^2) from PD to PI by using the fixed $\beta = 1.145$ and the five different parameterizations of spectral shape (Martin94, RLiu03, PengL03, Liu08, and LiuLi15), respectively. Black rectangles indicate the three sensitive regions with noticeable SW AIE.

The global/regional relative difference in SW AIE between the simulations using the spectral parameterization and using the fixed $\beta = 1.145$ denotes the impact of dispersion effect on SW AIE (bracketed percentages in Table 3). The larger the absolute value of the percentage, the stronger the dispersion effect and its impact on SW AIE. The negative percentage indicates that dispersion effect counteracts SW AIE (i.e., positive dispersion effect); while the positive percentage indicates that dispersion effect strengthens SW AIE (i.e., negative dispersion effect). The two parameterizations including dynamic factor (Liu08 and LiuLi15) have negative global dispersion effects, which are opposite to positive dispersion effect by applying simple $\beta - N_d$ relationships in previous GCMs. It again verifies non-negligible impact of cloud dynamic factors on the dispersion effect. Due to the large background value of β (1.18, which is close to the fixed $\beta = 1.145$) in PengL03 (Figure 2c1), the impacts of its dispersion effect on AIE are quite weak in all regions (Table 3).

Table 3 shows that the global dispersion effects caused by the five parameterizations modify SW AIE by -10% (counteract) to 13% (strengthen). However, it exhibits noticeably spatial inhomogeneity. Global land has overall stronger dispersion effect than ocean regions, possibly due to the stronger response of cloud properties to the change in droplet number over land. Over the sensitive regions, dispersion effects are generally stronger than global ocean. Because the vast open ocean areas in the Southern Hemisphere have relatively clean environment with few droplets but abundant moisture; thus, clouds have potentially small change in

Table 3

Simulated SW AIE (Unit is W/m^2) With the Fixed $\beta = 1.145$ and the Five Different Parameterizations of Spectral Shape (Martin94, RLiu03, PengL03, Liu08, and LiuLi15) as Averages Over the Globe, Over Land, Over Ocean, and Over the Three Sensitive Regions Including Southeast Asia, North Pacific Region, and West Coast of South America

	Fixed	Martin94	RLiu03	PengL03	Liu08	LiuLi15
Globe	-1.66	-1.57(-5.42%)	-1.5(-9.64%)	-1.67(0.6%)	-1.78(7.23%)	-1.87(12.65%)
Land	-1.5	-1.39(-7.33%)	-1.35(-10%)	-1.53(2%)	-1.59(6%)	-1.81(20.67%)
Ocean	-1.74	-1.67(-4.02%)	-1.59(-8.62%)	-1.75(0.57%)	-1.87(7.47%)	-1.89(8.62%)
Sensitive regions	-6.41	-5.98(-6.71%)	-5.71(-10.92%)	-6.44(0.47%)	-6.00(-6.4%)	-7.09(10.61%)

Note. Number in bracket is the relative difference in SW AIE between the simulations using the spectral parameterization and using the fixed $\beta = 1.145$.

Table 4

Response of Shortwave Cloud Forcing ($R_{sw,TOA}$), Liquid Water Path (L), Effective Radius of Cloud Droplets ($R_{e,top}$) and Effective Radius Factor (β_{top}) to Changes in Cloud Droplet Number Concentrations ($N_{d,pro}$) From PD to PI by Using Different Spectral Parameterizations, and Averaging Over the Three Sensitive Regions Including Southeast Asia, North Pacific Region, and West Coast of South America

	Fixed	Martin94	RLiu03	PengL03	Liu08	LiuLi15
$\Delta \ln \bar{R}_{sw,TOA} / \Delta \ln \bar{N}_{d,pro}$	0.213	0.179	0.178	0.207	0.182	0.236
$\Delta \ln \bar{L} / \Delta \ln \bar{N}_{d,pro}$	0.33	0.27	0.25	0.31	0.32	0.37
$-\Delta \ln \bar{R}_{e,top} / \Delta \ln \bar{N}_{d,pro}$	0.26	0.24	0.21	0.22	0.20	0.19
$\Delta \ln \bar{\beta}_{top} / \Delta \ln \bar{N}_{d,pro}$	—	0.0170	0.0174	0.0171	0.0172	0.0157

droplet number (lack of perturbation of pollution) and weak response of droplet spectral shape (all droplets can grow by condensation with sufficient moisture, thus will have little impact on the spectral width). To further understand the physical mechanism of the five spectral parameterizations, we decompose the response of shortwave cloud forcing in the sensitive regions for a further analysis, as both aerosol pollution and moisture have considerable impacts on cloud properties in these regions.

As mentioned in section 2.2.4, $\Delta \ln \bar{R}_{sw,TOA} / \Delta \ln \bar{N}_{d,pro}$ represents the change of shortwave cloud forcing with the perturbed cloud droplet number concentration as aerosol changes from PD to PI, denoting the response of shortwave cloud forcing (Ghan et al., 2016). According to Equation 8, Table 4 shows the contribution to shortwave forcing response ($\Delta \ln \bar{R}_{sw,TOA} / \Delta \ln \bar{N}_{d,pro}$) by individual cloud microphysical quantity: liquid water path response ($\Delta \ln \bar{L} / \Delta \ln \bar{N}_{d,pro}$), droplet effective radius response ($\Delta \ln \bar{R}_{e,top} / \Delta \ln \bar{N}_{d,pro}$), and effective radius factor response ($\Delta \ln \bar{\beta}_{top} / \Delta \ln \bar{N}_{d,pro}$). Negative $\Delta \ln \bar{R}_{e,top} / \Delta \ln \bar{N}_{d,pro}$ indicates that enhanced droplet number leads to reduced droplet size. Positive $\Delta \ln \bar{\beta}_{top} / \Delta \ln \bar{N}_{d,pro}$ and $\Delta \ln \bar{L} / \Delta \ln \bar{N}_{d,pro}$ indicate that enhanced droplet number results in a broader spectrum of cloud droplets and higher liquid water path of cloud in model. Note that cloud droplet number and size, together with the liquid water amount in cloud, determine the droplet size-number spectral shape in MG1.5. Additionally, these microphysical quantities are also correlated complexly to cloud dynamic factor, such as updraft. Therefore, the respect contributions from the decomposed response of cloud droplet size, spectral shape, and liquid water amount are not linearly additive to fully explain the shortwave forcing response in Table 4.

Figure 6 plots the items in Table 4 but normalized by the mean of five (six) simulations with different spectral shape parameterization (and with the fixed β). Higher values in Figure 6 indicate that the decomposed response is relatively stronger among the five (six) simulations. Those parameterizations only considered N_d in formulas (Martin94 [red line], RLiu03 [orange line], and PengL03 [green line]) show similar performances (relatively smaller $\Delta \ln \bar{L} / \Delta \ln \bar{N}_{d,pro}$ and larger $-\Delta \ln \bar{R}_{e,top} / \Delta \ln \bar{N}_{d,pro}$, and almost identical $\Delta \ln \bar{\beta}_{top} / \Delta \ln \bar{N}_{d,pro}$).

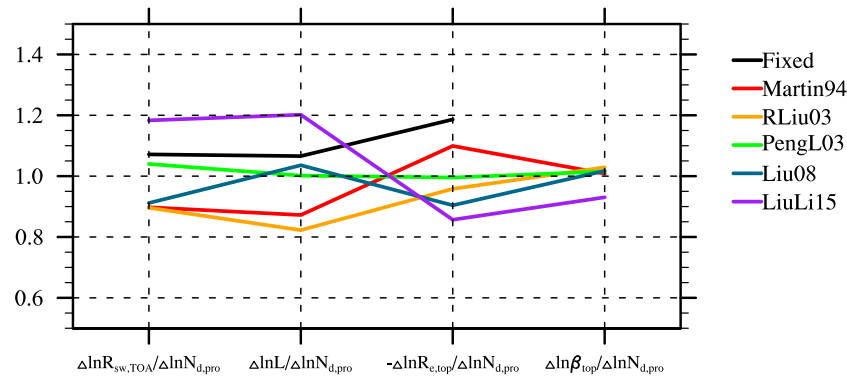


Figure 6. The items are shown in Table 4 but normalized by the mean of five (six) simulations with different spectral shape parameterization (and with the fixed β). Red, Martin94; orange, RLiu03; green, PengL03; blue, Liu08; and purple, LiuLi15.

$\ln\bar{N}_{d,\text{pro}}$) in Figure 6. For Liu08 (blue line), liquid water path is explicitly included in the spectral shape parameterization, and thus, relatively larger $\Delta\ln\bar{L}/\Delta\ln\bar{N}_{d,\text{pro}}$ and smaller $-\Delta\ln\bar{R}_{e,\text{top}}/\Delta\ln\bar{N}_{d,\text{pro}}$ are shown among the five parameterizations. LiuLi15 is derived from the theory of droplet condensational growth (Liu & Li, 2015), and several factors can modify the cloud droplet spectrum, such as supersaturation, water vapor condensation rate (dQ_c/dt in Table 1), droplet number concentration, and liquid water content. The impacts of different factors on droplet spectrum can offset each other (Figure 1). As a result, LiuLi15 (purple line) shows the smallest $\Delta\ln\bar{\beta}_{\text{top}}/\Delta\ln\bar{N}_{d,\text{pro}}$ compared to the other four parameterizations (Figure 6). It indicates that LiuLi15 has the mostly narrowed cloud droplet spectrum when droplet number increases, and largest $\Delta\ln\bar{L}/\Delta\ln\bar{N}_{d,\text{pro}}$ as droplets are hard to convert into raindrops with narrow spectrum. The narrowest size distribution is likely due to the assumption of the adiabatic condensation in the LiuLi15 formulation.

4. Concluding Remarks

In this study, four empirical and one semi-analytical parameterizations of cloud droplet spectral shape are implemented and examined in CAM5.3. The cloud microphysical scheme is double called in each simulation to output the instantaneous difference between the five parameterizations. Compared to Martin94 (the default spectral shape parameterization in CAM5.3), RLiu03, PengL03, and LiuLi15 show wider cloud droplet spectrum and faster autoconversion rate, but Liu08 shows a narrower droplet spectrum and slower autoconversion rate. All the spectral parameterizations have noticeable impacts on cloud microphysical properties (e.g., the changes in droplet number concentration, liquid water path, and droplet effective radius) but have limited impacts on the simulated shortwave cloud radiative forcing and total precipitation. Replacing the default spectral parameterization with the alternative one cannot fill the gap between the simulated cloud properties and satellite observations.

From PD to PI, SW AIEs estimated from the simulations with a fixed $\beta = 1.145$ and with the five spectral parameterizations are analyzed. The global dispersion effects caused by the five parameterizations modify SW AIE by -10% (counteract) to 13% (strengthen). The two parameterizations including dynamic factor (Liu08 and LiuLi15) have negative global dispersion effects, which are opposite to positive dispersion effect by applying simple $\beta - N_d$ relationships in previous GCMs. Our model results exhibit noticeably spatial inhomogeneity in simulated AIEs and dispersion effects. In the AIE sensitive regions (Southeast Asia, North Pacific, and West Coast of South America), we decompose the response of shortwave cloud forcing to the change in cloud droplet number from PD to PI, investigating the responses of cloud microphysical quantities in each spectral parameterization. Our results show that the semi-analytical parameterization (LiuLi15) has the strongest liquid water path response ($\Delta\ln\bar{L}/\Delta\ln\bar{N}_{d,\text{pro}}$) but the weakest effective radius response and dispersion response ($-\Delta\ln\bar{R}_{e,\text{top}}/\Delta\ln\bar{N}_{d,\text{pro}}$ and $\Delta\ln\bar{\beta}_{\text{top}}/\Delta\ln\bar{N}_{d,\text{pro}}$).

Several points are noteworthy. First, in state-of-the-art GCMs, two-moment microphysical scheme is generally applied for simulating the large-scale stratus/stratiform clouds. Although the shape of cloud droplet spectrum has non-negligible impact on cloud properties, employing the three-moment microphysical scheme remains computationally expensive (Milbrandt & Yau, 2005a, 2005b) in GCM (yet applicable in weather forecast model). Parameterization of cloud droplet spectral shape remains an attractive alternative. The notable uncertainties caused by the dispersion effect in various properties including AIE call for more studies to improve the parameterization. Second, most spectral parameterizations are empirically derived by fitting to the relationship between spectral shape parameter and cloud droplet number and/or liquid water content. The only semi-analytical expression (LiuLi15) is derived under the assumption of adiabatic clouds. However, it has been long recognized that turbulent entrainment-mixing processes in nonadiabatic clouds can affect the droplet spectrum (Bera et al., 2016; Chandrakar et al., 2018a; 2018b; Guo et al., 2018), which should be considered in future work on spectral parameterizations. Third, the autoconversion scheme used in this study only includes the relative dispersion in rate function but not in threshold function. A more general scheme for autoconversion (Liu et al., 2007) explicitly accounts for the relative dispersion in both rate function and threshold function. By applying different autoconversion schemes into GCM, the impact of dispersion effect on cloud-to-rain conversion can be investigated (e.g., Guo et al., 2008, using a LES model) in future study, helping to better understand the aerosol-cloud interaction.

Last but not the least, all the simulations in this study are performed in transient historical run with realistic SST and sea ice, which only reflect the rapid adjustments of the atmosphere. Noting that the sensitive regions for dispersion effect and SW AIE are mostly over oceans, it would be interesting to run the fully coupled atmosphere–ocean model and investigate the feedback effects of different spectral parameterizations on climate in future works.

Data Availability Statement

The source code for CAM5.3 is distributed through a public Subversion code repository. This code can be checked out using Subversion client software, such as the command tool svn, or simply view the version with a web browser https://svn-ccsm-models.cgd.ucar.edu/cesm1/release_tags/cesm1_2_1/. The input data necessary to run CAM5.3 is made available at <https://svn-ccsm-inputdata.cgd.ucar.edu/trunk/inputdata/>. CERES data are available in https://ceres.larc.nasa.gov/order_data.php. The products of SSF1deg-Level 3 Terra Edition 4A are used for 2001–2005 monthly mean of Cloud Visible Optical Depth, Liquid Water Path and Water Particle Radius at 3.7 μm . Shortwave cloud forcing at the top of the atmosphere (TOA) is calculated by all-sky and clear-sky shortwave flux from products of EBAF-TOA-Level 3b. The spatial resolution is $1^\circ \times 1^\circ$ global grid. MODIS, GPCP, and TRMM data are available in <https://giovanni.gsfc.nasa.gov/giovanni/>. The $1^\circ \times 1^\circ$ 2001–2005 monthly Liquid Water Cloud Effective Particle Radius is used by MODIS Terra product (MOD08_M3 v6.1). GPCPMON v3.0 (combined satellite-gauge precipitation monthly $0.5^\circ \times 0.5^\circ$) and TRMM_3B42_v7 (TRMM Rainfall Estimate L3 3 h $0.25^\circ \times 0.25^\circ$ V7) are used for comparison of precipitation. ISCCP D2 is used for $2.5^\circ \times 2.5^\circ$ 2001–2005 monthly mean cloud water path, and data are available in the following website <https://isccp.giss.nasa.gov/products/dataview.html>.

Acknowledgments

Yiran Peng, Minqi Wang, and Zengyuan Guo were supported by National Important Project of the Ministry of Science and Technology in China (grant 2017YFC1501404) and National Natural Science Foundation of China (Grants 41605106, 41775137, and 71690243). Yangang Liu is supported by the U.S. Department of Energy's Atmospheric System Research (ASR) program. Yu Liu is supported by the National Key Research and Development Program of China (Grant 2017YFA0603501).

References

- Abdul-Razzak, H., & Ghan, S. J. (2000). A parameterization of aerosol activation 2. Multiple aerosol types. *Journal of Geophysical Research: Atmospheres*, 105, 6837–6844. <https://doi.org/10.1029/1999JD901161>
- Bera, S., Pandithurai, G., & Prabha, T. V. (2016). Entrainment and droplet spectral characteristics in convective clouds during transition to monsoon. *Atmospheric Science Letters*, 17(4), 286–293. <https://doi.org/10.1002/asl.293>
- Chandrakar, K. K., Cantrell, W., Kostinski, A. B., & Shaw, R. A. (2018a). Dispersion aerosol indirect effect in turbulent clouds: Laboratory measurements of effective radius. *Geophysical Research Letters*, 45, 10,738–10,745. <https://doi.org/10.1029/2018GL079194>
- Chandrakar, K. K., Cantrell, W., & Shaw, R. A. (2018b). Influence of turbulent fluctuations on cloud droplet size dispersion and aerosol indirect effects. *Journal of the Atmospheric Sciences*, 75(9), 3191–3209. <https://doi.org/10.1175/jas-d-18-0006.1>
- Chen, J. Y., Liu, Y. G., Zhang, M. H., & Peng, Y. R. (2016). New understanding and quantification of the regime dependence of aerosol–cloud interaction for studying aerosol indirect effects. *Geophysical Research Letters*, 43, 1780–1787. <https://doi.org/10.1002/2016GL067683>
- Chen, J. Y., Liu, Y. G., Zhang, M. H., & Peng, Y. R. (2018). Height dependency of aerosol–cloud interaction regimes. *Journal of Geophysical Research: Atmospheres*, 123, 491–506. <https://doi.org/10.1002/2017JD027431>
- Forster, P. M., Richardson, T., Maycock, A. C., Smith, C. J., Samset, B. H., Myhre, G., et al. (2016). Recommendations for diagnosing effective radiative forcing from climate models for CMIP6. *Journal of Geophysical Research: Atmospheres*, 121, 12,460–12,475. <https://doi.org/10.1002/2016JD025320>
- Gettelman, A., Morrison, H., & Ghan, S. J. (2008). A new two-moment bulk stratiform cloud microphysics scheme in the community atmosphere model, version 3 (CAM3). Part II: Single-column and global results. *Journal of Climate*, 21(15), 3660–3679. <https://doi.org/10.1175/2008jcli2116.1>
- Ghan, S., Wang, M., Zhang, S., Ferrachat, S., Gettelman, A., Griesfeller, J., et al. (2016). Challenges in constraining anthropogenic aerosol effects on cloud radiative forcing using present-day spatiotemporal variability. *Proceedings of the National Academy of Sciences of the United States of America*, 113(21), 5804–5811. <https://doi.org/10.1073/pnas.1514036113>
- Guo, H., Liu, Y., & Penner, J. E. (2008). Does the threshold representation associated with the autoconversion process matter? *Atmospheric Chemistry and Physics*, 8(5), 1225–1230. <https://doi.org/10.5194/acp-8-1225-2008>
- Guo, X. H., Lu, C. S., Zhao, T. L., Liu, Y. G., Zhang, G. J., & Luo, S. (2018). Observational study of the relationship between entrainment rate and relative dispersion in deep convective clouds. *Atmospheric Research*, 199, 186–192. <https://doi.org/10.1016/j.atmosres.2017.09.013>
- Iacono, M. J., Delamere, J. S., Mlawer, E. J., Shephard, M. W., Clough, S. A., & Collins, W. D. (2008). Radiative forcing by long-lived greenhouse gases: Calculations with the AER radiative transfer models. *Journal of Geophysical Research*, 113, D13103. <https://doi.org/10.1029/2008JD009944>
- Khairoutdinov, M., & Kogan, Y. (2000). A new cloud physics parameterization in a large-eddy simulation model of marine stratocumulus. *Monthly Weather Review*, 128(1), 229–243. [https://doi.org/10.1175/1520-0493\(2000\)128<0229:Anccpi>2.0.Co;2](https://doi.org/10.1175/1520-0493(2000)128<0229:Anccpi>2.0.Co;2)
- Komurcu, M., Storelvmo, T., Tan, I., Lohmann, U., Yun, Y. X., Penner, J. E., et al. (2014). Intercomparison of the cloud water phase among global climate models. *Journal of Geophysical Research: Atmospheres*, 119, 3372–3400. <https://doi.org/10.1002/2013JD021119>
- Kooperman, G. J., Pritchard, M. S., Ghan, S. J., Wang, M., Somerville, R. C. J., & Russell, L. M. (2012). Constraining the influence of natural variability to improve estimates of global aerosol indirect effects in a nudged version of the Community Atmosphere Model 5. *Journal of Geophysical Research*, 117, D23204. <https://doi.org/10.1029/2012JD018588>
- Liu, X., Easter, R. C., Ghan, S. J., Zaveri, R., Rasch, P., Shi, X., et al. (2012). Toward a minimal representation of aerosols in climate models: Description and evaluation in the Community Atmosphere Model CAM5. *Geoscientific Model Development*, 5(3), 709–739. <https://doi.org/10.5194/gmd-5-709-2012>
- Liu, Y., & Li, W. L. (2015). A method for solving relative dispersion of the cloud droplet spectra. *Science China Earth Sciences*, 58(6), 929–938. <https://doi.org/10.1007/s11430-015-5059-9>

- Liu, Y. G., & Daum, P. H. (2000). Spectral dispersion of cloud droplet size distributions and the parameterization of cloud droplet effective radius. *Geophysical Research Letters*, 27, 1903–1906. <https://doi.org/10.1029/1999GL011011>
- Liu, Y. G., & Daum, P. H. (2002). Anthropogenic aerosols indirect warming effect from dispersion forcing. *Nature*, 419(6907), 580–581. <https://doi.org/10.1038/419580a>
- Liu, Y. G., & Daum, P. H. (2004). Parameterization of the autoconversion process. Part I: Analytical formulation of the Kessler-type parameterizations. *Journal of the Atmospheric Sciences*, 61(13), 1539–1548. [https://doi.org/10.1175/1520-0469\(2004\)061<1539:Potapi>2.0.Co;2](https://doi.org/10.1175/1520-0469(2004)061<1539:Potapi>2.0.Co;2)
- Liu, Y. G., Daum, P. H., Guo, H., & Peng, Y. R. (2008). Dispersion bias, dispersion effect, and the aerosol-cloud conundrum. *Environmental Research Letters*, 3(4), 8. <https://doi.org/10.1088/1748-9326/3/4/045021>
- Liu, Y. G., Daum, P. H., & Lu, C. S. (2014). Comment on “Cloud droplet spectral width relationship to CCN spectra and vertical velocity” by Hudson et al. *Journal of Geophysical Research: Atmospheres (USA)*, 119, 1874–1877. <https://doi.org/10.1002/2012jd019207>
- Liu, Y. G., Daum, P. H., & McGraw, R. L. (2005). Size truncation effect, threshold behavior, and a new type of autoconversion parameterization. *Geophysical Research Letters*, 32, L11811. <https://doi.org/10.1029/2005GL022636>
- Liu, Y. G., Daum, P. H., McGraw, R. L., Miller, M. A., & Niu, S. J. (2007). Theoretical expression for the autoconversion rate of the cloud droplet number concentration. *Geophysical Research Letters*, 34, L16821. <https://doi.org/10.1029/2007GL030389>
- Liu, Y. G., Daum, P. H., & Yum, S. S. (2006). Analytical expression for the relative dispersion of the cloud droplet size distribution. *Geophysical Research Letters*, 33, L02810. <https://doi.org/10.1029/2005GL024052>
- Lu, M.-L., Conant, W. C., Jonsson, H. H., Varutbangkul, V., Flagan, R. C., & Seinfeld, J. H. (2007). The Marine Stratus/Stratocumulus Experiment (MASE): Aerosol-cloud relationships in marine stratocumulus. *Journal of Geophysical Research*, 112, D10209. <https://doi.org/10.1029/2006JD007985>
- Ma, J. Z., Chen, Y., Wang, W., Yan, P., Liu, H. J., Yang, S. Y., et al. (2010). Strong air pollution causes widespread haze-clouds over China. *Journal of Geophysical Research*, 115, D18204. <https://doi.org/10.1029/2009JD013065>
- Martin, G. M., Johnson, D. W., & Spice, A. (1994). The measurement and parameterization of effective radius of droplets in the warm stratocumulus clouds. *Journal of the Atmospheric Sciences*, 51(13), 1823–1842. [https://doi.org/10.1175/1520-0469\(1994\)051<1823:Tmapoe>2.0.Co;2](https://doi.org/10.1175/1520-0469(1994)051<1823:Tmapoe>2.0.Co;2)
- Martins, J. A., & Dias, M. (2009). The impact of smoke from forest fires on the spectral dispersion of cloud droplet size distributions in the Amazonian region. *Environmental Research Letters*, 4(1), 8. <https://doi.org/10.1088/1748-9326/4/1/015002>
- Milbrandt, J. A., & Yau, M. K. (2005a). A multimoment bulk microphysics parameterization. Part I: Analysis of the role of the spectral shape parameter. *Journal of the Atmospheric Sciences*, 62(9), 3051–3064. <https://doi.org/10.1175/jas3534.1>
- Milbrandt, J. A., & Yau, M. K. (2005b). A multimoment bulk microphysics parameterization. Part II: A proposed three-moment closure and scheme description. *Journal of the Atmospheric Sciences*, 62(9), 3065–3081. <https://doi.org/10.1175/jas3535.1>
- Mlawer, E. J., Taubman, S. J., Brown, P. D., Iacono, M. J., & Clough, S. A. (1997). Radiative transfer for inhomogeneous atmospheres: RRTM, a validated correlated-k model for the longwave. *Journal of Geophysical Research: Atmospheres*, 102, 16,663–16,682. <https://doi.org/10.1029/97JD00237>
- Morrison, H., & Gettelman, A. (2008). A new two-moment bulk stratiform cloud microphysics scheme in the community atmosphere model, version 3 (CAM3). Part I: Description and numerical tests. *Journal of Climate*, 21(15), 3642–3659. <https://doi.org/10.1175/2008jcli2105.1>
- Neale, R. B., Chen, C.-C., Gettelman, A., Lauritzen, P. H., Park, S., Williamson, D. L., et al. (2012). *Description of the NCAR community atmosphere model (CAM 5.0)*, NCAR Tech. (Note NCAR/TN-485+STR, pp. 1–289). Boulder, CO: National Center for Atmospheric Research.
- Painemal, D., & Zuidema, P. (2011). Assessment of MODIS cloud effective radius and optical thickness retrievals over the Southeast Pacific with VOCALS-REx in situ measurements. *Journal of Geophysical Research*, 116, D24206. <https://doi.org/10.1029/2011JD016155>
- Peng, Y. R., & Lohmann, U. (2003). Sensitivity study of the spectral dispersion of the cloud droplet size distribution on the indirect aerosol effect. *Geophysical Research Letters*, 30(10), 1507. <https://doi.org/10.1029/2003GL017192>
- Rotstayn, L. D., & Liu, Y. G. (2003). Sensitivity of the first indirect aerosol effect to an increase of cloud droplet spectral dispersion with droplet number concentration. *Journal of Climate*, 16(21), 3476–3481. [https://doi.org/10.1175/1520-0442\(2003\)016<3476:Sotfia>2.0.Co;2](https://doi.org/10.1175/1520-0442(2003)016<3476:Sotfia>2.0.Co;2)
- Rotstayn, L. D., & Liu, Y. G. (2009). Cloud droplet spectral dispersion and the indirect aerosol effect: Comparison of two treatments in a GCM. *Geophysical Research Letters*, 36, L10801. <https://doi.org/10.1029/2009GL038216>
- Twomey, S. (1991). Aerosols, clouds and radiation. *Atmospheric Environment Part a-General Topics*, 25(11), 2435–2442. [https://doi.org/10.1016/0960-1686\(91\)90159-5](https://doi.org/10.1016/0960-1686(91)90159-5)
- Wang, Y., Niu, S. J., Lu, C. S., Liu, Y. G., Chen, J. Y., & Yang, W. X. (2019). An observational study on cloud spectral width in North China. *Atmosphere*, 10(3), 14. <https://doi.org/10.3390/atmos10030109>
- Xie, X. N., Liu, X. D., Peng, Y. R., Wang, Y., Yue, Z. G., & Li, X. Z. (2013). Numerical simulation of clouds and precipitation depending on different relationships between aerosol and cloud droplet spectral dispersion. *Tellus Series B: Chemical and Physical Meteorology*, 65(1), 19054. <https://doi.org/10.3402/tellusb.v65i0.19054>
- Xie, X. N., Zhang, H., Liu, X. D., Peng, Y. R., & Liu, Y. G. (2017). Sensitivity study of cloud parameterizations with relative dispersion in CAM5.1: Impacts on aerosol indirect effects. *Atmospheric Chemistry and Physics*, 17(9), 5877–5892. <https://doi.org/10.5194/acp-17-5877-2017>
- Xie, X. N., Zhang, H., Liu, X. D., Peng, Y. R., & Liu, Y. G. (2018). Role of microphysical parameterizations with droplet relative dispersion in IAP AGCM 4.1. *Advances in Atmospheric Sciences*, 35(2), 248–259. <https://doi.org/10.1007/s00376-017-7083-5>
- Yum, S. S., & Hudson, J. G. (2005). Adiabatic predictions and observations of cloud droplet spectral broadness. *Atmospheric Research*, 73(3–4), 203–223. <https://doi.org/10.1016/j.atmosres.2004.10.006>
- Zhang, K., O'Donnell, D., Kazil, J., Stier, P., Kinne, S., Lohmann, U., et al. (2012). The global aerosol-climate model ECHAM-HAM, version 2: Sensitivity to improvements in process representations. *Atmospheric Chemistry and Physics*, 12(19), 8911–8949. <https://doi.org/10.5194/acp-12-8911-2012>
- Zhao, C., Tie, X., Brasseur, G., Noone, K. J., Nakajima, T., Zhang, Q., et al. (2006). Aircraft measurements of cloud droplet spectral dispersion and implications for indirect aerosol radiative forcing. *Geophysical Research Letters*, 33, L16809. <https://doi.org/10.1029/2006GL026653>
- Zhao, X. P., Liu, Y. G., Yu, F. Q., & Heidinger, A. K. (2018). Using long-term satellite observations to identify sensitive regimes and active regions of aerosol indirect effects for liquid clouds over global oceans. *Journal of Geophysical Research: Atmospheres*, 123, 457–472. <https://doi.org/10.1002/2017JD027187>